2017 IEEE Conference on Control Technology and Applications (CCTA)
August 27-30, 2017. Kohala Coast, Hawai'i, USA

Maneuvering and Stabilizing Control of a Quadrupedal Robot using a Serpentine Robotic Tail

William S. Rone, *Student Member, IEEE*, and Pinhas-Ben-Tzvi, *Senior Member, IEEE*

***Abstract*—This paper analyzes the control of a mobile robotic system that utilizes a serpentine robotic tail to assist in the maneuvering and stabilization of quadrupedal locomotion. The goal of this research is to reduce the design and control complexity required in the robot's legs by providing a separate mechanism to help the mobile robot steer and recover from disturbances. The design and dynamic models for a quadrupedal robotic platform's yaw, pitch and roll are presented, along with the design and dynamic model of the roll-revolute-revolute robotic tail (R3-RT). Dynamic tail configuration controllers are designed to enable different system functionalities, including yaw-angle turning and pitch/roll-angle stabilization. Case studies are simulated in MATLAB to demonstrate the proposed functionalities.**

I. Introduction

A fruitful approach in the design of robotic systems is to look to nature for inspiration. Although biomimicry has recently become a particularly intense research focus, the earliest legged robots attempted to recreate how humans and animals move [1], instead of using wheels or tracks. Efforts to enhance robotic legged locomotion have also looked to nature. Torso and upper-body maneuvering [2] to stabilize bipeds further adapts anatomy into robotic systems. Degrees-of-freedom (DOF) between the fore and aft legs in quadrupeds [3] mimic the natural flexibility of a spine.

Another source of inspiration for enhancing legged locomotion is animals' tails. Tail function differs greatly between animals [4], ranging from balance in a house cat [5] to assisting turning in a cheetah [6] to self-supporting its weight in a kangaroo [7]. Previous work in robotic tails has focused primarily on single-mass pendulum-type structures rotating in fixed planes to perform a specific function. Single-DOF tails operating in in the yaw [8], pitch [9], [10], and roll [11] directions have been demonstrated, along with two-DOF tails in the yaw-pitch [12] and roll-pitch [13] directions.

Beyond rigid pendulums, recent research has studied designs of more biomimetic tails [14]–[18]. This paper studies how the roll-revolute-revolute robotic tail (R3RT, [14]) can be used to assist the stabilization and maneuvering of a quadrupedal robot comprised of four Robotic Modular Leg (RMLeg) units [19]. This paper build on the author's work in [20] by considering pitch- and roll-angle stabilization alongside the yaw-angle maneuvering using the R3RT.

The paper is organized as follows: Section II presents the system design and dynamic models for the tail and quadruped. Section III discusses the yaw-, roll- and pitch-angle controllers used to maneuver or stabilize the quadruped. Section IV presents the results of the three case studies implemented using the system models and controllers. Section V concludes the paper and discusses future work.

* This material is based upon work supported by the National Science Foundation under Grant No. 1557312.

W. S. Rone and P. Ben-Tzvi are with Virginia Tech, Blacksburg, VA 24061 USA. (phone: 540-231-6938; fax: 540-231-9100; email: wsrone@vt.edu, bentzvi@vt.edu).

II. System Design and Model

This section presents the design of the quadruped with tail (II-A), and discusses the mathematical models used to calculate the tail loading from its trajectory (II-B), along with the models to simulate the quadruped for analyzing yaw-angle maneuvering (II-C), roll-angle stabilization (II-D) and pitch-angle stabilization (II-E).

A. Overall System Design

Figure 1 illustrates the overall system design comprised of four RMLeg units and an R3RT. The RMLeg unit [19] is a two-DOF leg that utilizes a pair of parallelogram four-bar mechanisms to hold the hip and foot links parallel as the foot moves relative to the hip. In this paper, the quadruped legs are held in fixed positions relative to their hip links to analyze the tail motion's impact on the overall system dynamics.

The R3RT [14] is a serpentine robotic structure comprised of a fixed housing, an actuation module, and 12 tail links, as shown in Figure 2. The fixed housing and actuation module are connected by a roll revolute joint, and the 12 tail links are connected to the actuation module and each other through pitch revolute joints. Thus, the R3RT bends in a rotating plane, generating spatial motion. As shown in Figures 1 and 2, the R3RT is arranged into two individually actuated bending segments, with two sets of six links coupled to bend together.

Redundancy in each 6 link segment is resolved using 5 gear pairs that constrain the segment motion such that the relative angle between each gear pair is equal. Thus, the six joint angles are all equal to one nominal value. A pair of antagonistically routed cables is used to actuate each

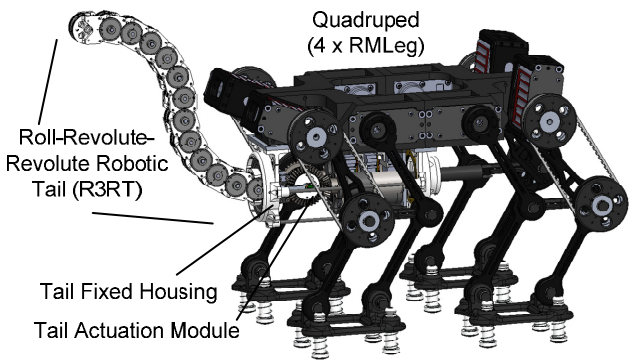

Figure 1. RMLeg Quadruped with R3RT.

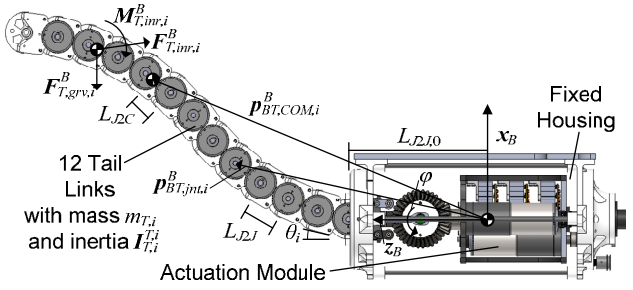

Figure 2. R3RT with relevant kinematic and loading parameters labeled.

segment, and the cables are routed along cylindrical surfaces to ensure equal extension/retraction of the cable pair. These cable pairs are connected to spools actuated by a gearmotor through a bevel gear transmission.

B. Tail Model

In this analysis, it will be assumed that the tail controller can prescribe desired joint angle trajectories to the R3RT. As discussed in section V, future work will address the inner-loop tail control required to map these desired trajectories into motor commands to implement the desired trajectory.

A kinematic model will be used to generate the tail trajectory similar to [20], [21]. The controller outputs in section III will prescribe joint angle trajectories, and the controllers will modify these trajectories based on system feedback such as system orientation and angular velocity. Therefore, this analysis assumes that the tail joint angle trajectories and their time derivatives are known.

The tail model in this section will be defined with respect to the tail base frame *B*, shown in Fig. 2. The frame *B* origin is coincident with the link 0 actuation module center of mass (COM). Frame *B* is also fixed to the quadruped, and the loading applied by the tail will be mapped into the quadruped frame in sections II-C,D,E. A vector superscript denotes the frame in which the vector is defined; if the superscript is omitted, it is defined with respect to the fixed global frame.

The tail link *i* orientations $\boldsymbol{R}^B_{BT,i}$ and angular velocities $\boldsymbol{\omega}^B_{BT,i}$ with respect to frame *B* are defined in Eq. 1, where φ is the link 0 roll angle, θ_i is the pitch joint *i* angle, $\boldsymbol{R}_Y(\cdot)$ and $\boldsymbol{R}_Z(\cdot)$ are y- and z-axes rotations, respectively, $\boldsymbol{y}^B_{T,i}$ and $\boldsymbol{z}^B_{T,i}$ are the tail link *i* frame y- and z-axis unit vectors, respectively, and $\dot{\varphi}$ denotes the first time derivative of φ.

$$\boldsymbol{R}^B_{BT,i}=\begin{cases}\boldsymbol{R}_Z(\varphi) & i=0\\ \boldsymbol{R}^B_{BT,i-1}\boldsymbol{R}_Y(\theta_i) & i\geq 1\end{cases},\quad \boldsymbol{\omega}^B_{BT,i}=\begin{cases}\dot{\varphi}\boldsymbol{z}^B_{T,i} & i=0\\ \boldsymbol{\omega}^B_{T,i-1}+\dot{\theta}_i\boldsymbol{y}^B_{T,i} & i\geq 1\end{cases} \quad (1)$$

The position $\boldsymbol{p}^B_{BT,jnt,i}$ from frame B to joint *i* is defined in Eq. 2, where $L_{JJ,0}$ is the distance between joints 1 and 2 and L_{JJ} is the distance between adjacent pitch joints. The center of mass (COM) positions $\boldsymbol{p}^B_{BT,COM,i}$ are defined in Eq. 3, where L_{JC} is the distance between a link's pitch joint and COM.

$$\boldsymbol{p}^B_{BT,jnt,i}=\begin{cases}\boldsymbol{0} & i=0\\ L_{JJ,0}\boldsymbol{z}^B_{BT,i-1} & i=1\\ \boldsymbol{p}^B_{jnt,i-1}+L_{JJ}\boldsymbol{z}^B_{BT,i-1} & i\geq 2\end{cases} \quad (2)$$

$$\boldsymbol{p}^B_{BT,COM,i}=\begin{cases}\boldsymbol{0} & i=0\\ \boldsymbol{p}^B_{BT,jnt,i}+L_{JC}\boldsymbol{z}^B_{BT,i} & i\geq 1\end{cases} \quad (3)$$

The angular accelerations $\boldsymbol{\alpha}^B_{BT,i}$ and linear velocities and accelerations $\boldsymbol{v}^B_{BT,jnt,i}$, $\boldsymbol{v}^B_{BT,dsk,i}$, $\boldsymbol{a}^B_{BT,jnt,i}$ and $\boldsymbol{a}^B_{BT,dsk,i}$ are found by differentiating Eqs. 1-3.

Two sources of external loading affect the force and moment between the tail and quadruped: gravity and inertia, shown in Fig. 2. These loading effects act at the COM of each link, and their cumulative effect may be calculated at the frame B origin. The link *i* inertial loading consists of the inertial force $\boldsymbol{F}^B_{T,inr,i}$ and moment $\boldsymbol{M}^B_{T,inr,i}$ due to the tail link's motion. Since the tail joint angle trajectories are assumed to be prescribed, these loading effects may be directly calculated from model inputs, as shown in Eq. 4, where $m_{T,i}$ and $\boldsymbol{I}^B_{T,i}$ are the tail link *i* mass and inertia, respectively, and $\tilde{\boldsymbol{\omega}}\boldsymbol{I}\boldsymbol{\omega}$ denotes the cross product $\boldsymbol{\omega}\times\boldsymbol{I}\boldsymbol{\omega}$. The inertia $\boldsymbol{I}^B_{T,i}$ is calculated from the fixed body-frame inertia $\boldsymbol{I}^{T,i}_{T,i}$ using Eq. 5. The tail body gravitational loading $\boldsymbol{F}^B_{T,grv,i}$ changes with varying quad pitch and roll and will be defined in sections II-C through II-E for the specific module under consideration.

$$\boldsymbol{F}^B_{T,inr,i}=m_{T,i}\boldsymbol{a}^B_{BT,COM,i},\quad \boldsymbol{M}^B_{T,inr,i}=\boldsymbol{I}^B_{T,i}\boldsymbol{\alpha}^B_{BT,i}+\tilde{\boldsymbol{\omega}}^B_{BT,i}\boldsymbol{I}^B_{T,i}\boldsymbol{\omega}^B_{BT,i} \quad (4)$$

$$\boldsymbol{I}^B_{T,i}=\boldsymbol{R}^B_{T,i}\boldsymbol{I}^{T,i}_{T,i}\left(\boldsymbol{R}^B_{T,i}\right)^T \quad (5)$$

The net force $\boldsymbol{F}^B_{tail}$ and moment $\boldsymbol{M}^B_{tail}$ the tail applies on the quadruped are defined in Eq. 6. In addition, the effect of the tail's mass and inertia need to be accounted for in the quad model since the tail loading did not incorporate the quad's motion. Therefore, the tail's effective mass m_T and inertia $\boldsymbol{I}^B_T$ at the origin of frame *B* are defined in Eq. 7 using the parallel axis theorem, where $\mathbf{I}_3$ is the 3x3 identity matrix.

$$\begin{aligned}\boldsymbol{F}^B_{tail}&=\sum_{i=0}^{12}\left(\boldsymbol{F}^B_{T,inr,i}-\boldsymbol{F}^B_{T,grv,i}\right)\\ \boldsymbol{M}^B_{tail}&=\sum_{i=0}^{12}\left(\boldsymbol{M}^B_{T,inr,i}+\tilde{\boldsymbol{p}}^B_{BT,COM,i}\left(\boldsymbol{F}^B_{T,inr,i}-\boldsymbol{F}^B_{T,grv,i}\right)\right)\end{aligned} \quad (6)$$

$$m_T=\sum_{i=0}^{12}\left(m_{T,i}\right),\quad \boldsymbol{I}^B_T=\sum_{i=0}^{12}\left(\boldsymbol{I}^B_{T,i}+m_{T,i}\left(\begin{matrix}\left(\boldsymbol{p}^B_{BT,COM,i}\cdot\boldsymbol{p}^B_{BT,COM,i}\right)\mathbf{I}_3\\ +\boldsymbol{p}^B_{BT,COM,i}\otimes\boldsymbol{p}^B_{BT,COM,i}\end{matrix}\right)\right) \quad (7)$$

C. Quadrupedal Model – Yaw-Angle Rotation

For the yaw-angle rotation model used to study the tail's maneuvering capabilities, a cylindrical joint is used between the quad and ground, defined at the quad COM and allowing x-direction rotation (yaw) and displacement. For this joint, the quad's angular acceleration $\boldsymbol{\alpha}$ is defined in Eq. 8, along with the non-zero elements of $\boldsymbol{F}_{jnt}$ and $\boldsymbol{M}_{jnt}$. For this case, the quad's linear acceleration $\boldsymbol{a}=\boldsymbol{0}$ (ground contact maintained).

$$\boldsymbol{\alpha}=\begin{bmatrix}\alpha_x & 0 & 0\end{bmatrix}^T,\quad \begin{aligned}\boldsymbol{F}_{jnt}&=\begin{bmatrix}0 & F_{jnt,y} & F_{jnt,z}\end{bmatrix}^T\\ \boldsymbol{M}_{jnt}&=\begin{bmatrix}0 & M_{jnt,y} & M_{jnt,z}\end{bmatrix}^T\end{aligned} \quad (8)$$

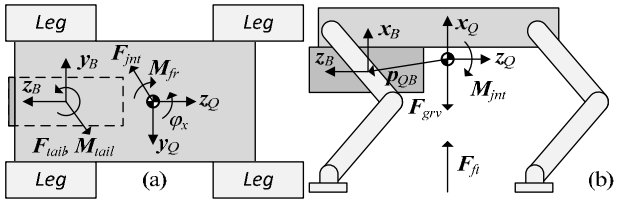

Figure 3. Yaw-angle model free-body diagram: (a) top view, (b) side view. The tail is not shown as its loading effect are captured by $\boldsymbol{F}_{tail}$ and $\boldsymbol{M}_{tail}$ and its mass and inertia are captured in m and $\boldsymbol{I}$.

Figure 3 illustrates the free-body diagram for the yaw-angle rotation quadruped model, where $\boldsymbol{F}_{grv}$ is the quad's gravitational loading, $\boldsymbol{F}_{ft}$ is the net force due to the feet supporting the quad, and $\boldsymbol{M}_{fr}$ is the net friction moment due to foot contact. The governing equations of motion relative to the quad COM are defined in Eqs. 9 and 10, where m is the system mass, $\boldsymbol{I}$ is the system inertia, and $\boldsymbol{p}_{QB}$ is the tail base position relative to the quad COM.

$$m\boldsymbol{a} = \boldsymbol{0} = \boldsymbol{F}_{jnt} + \boldsymbol{F}_{ft} + \boldsymbol{F}_{tail} + \boldsymbol{F}_{grv} \tag{9}$$

$$\boldsymbol{I}\boldsymbol{\alpha} = \boldsymbol{M}_{jnt} + \boldsymbol{M}_{fr} + \boldsymbol{M}_{tail} + \tilde{\boldsymbol{p}}_{QB}\boldsymbol{F}_{tail} \tag{10}$$

To define $\boldsymbol{I}$, $\boldsymbol{F}_{tail}$, $\boldsymbol{M}_{tail}$ and $\boldsymbol{p}_{tail}$, a quadruped kinematic model is needed. During the simulation, the system will rotate φ_x relative to the ground, resulting in a quad rotation matrix $\boldsymbol{R}_Q$ defined in Eq. 11, where $\boldsymbol{R}_X(\cdot)$ is the x-axis rotation. Equation 11 also defines the orientations of frame B with respect to the quad frame ($\boldsymbol{R}_B^Q$) and ground ($\boldsymbol{R}_B$).

$$\boldsymbol{R}_Q = \boldsymbol{R}_X(\varphi_x), \quad \boldsymbol{R}_B^Q = \boldsymbol{R}_X(180^\circ), \quad \boldsymbol{R}_B = \boldsymbol{R}_Q\boldsymbol{R}_B^Q \tag{11}$$

Using these frames, $\boldsymbol{F}_{tail}$, $\boldsymbol{M}_{tail}$ and $\boldsymbol{p}_{QB}$ can be defined in Eq. 12, where $\boldsymbol{p}_{QT}^Q$ is the position vector from the quad frame origin to the tail frame origin.

$$\boldsymbol{F}_{tail} = \boldsymbol{R}_B\boldsymbol{F}_{tail}^B, \quad \boldsymbol{M}_{tail} = \boldsymbol{R}_B\boldsymbol{M}_{tail}^B, \quad \boldsymbol{p}_{QB} = \boldsymbol{R}_Q\boldsymbol{p}_{QB}^Q \tag{12}$$

Because the section II-B tail model does not account for the quad's motion, the inertia terms in Eqs. 9 and 10 should include the tail inertia. Equation 13 defines m and $\boldsymbol{I}$, where m_Q and $\boldsymbol{I}_Q^Q$ are the quad mass and inertia.

$$\begin{aligned} &m = m_Q + m_T, \\ &\boldsymbol{I} = \boldsymbol{R}_Q\boldsymbol{I}_Q^Q(\boldsymbol{R}_Q)^T + \boldsymbol{R}_B\boldsymbol{I}_T^B(\boldsymbol{R}_B)^T + m_T\left(\boldsymbol{p}_{QB}\cdot\boldsymbol{p}_{QB}\mathbf{I}_3 + \boldsymbol{p}_{QB}\otimes\boldsymbol{p}_{QB}\right) \end{aligned} \tag{13}$$

For this case, $\boldsymbol{F}_{grv}$ and $\boldsymbol{F}_{T,grv,i}^B$ are invariant to φ_x and are defined by Eq. 14, where g is gravitational acceleration.

$$\boldsymbol{F}_{grv} = -m_Q g\boldsymbol{x}, \quad \boldsymbol{F}_{T,grv,i}^B = -m_{T,i}g(\boldsymbol{R}_B)^T\boldsymbol{x} \tag{14}$$

The net foot force $\boldsymbol{F}_{ft} = [F_{ft,x} \;\; 0 \;\; 0]^T$ represents the sum of the x-direction forces supporting the quad from the ground. This loading opposes the net x-direction gravity and tail forces. However, the individual foot forces also produce friction opposing net system rotation φ_x, manifested in $\boldsymbol{M}_{fr}$.

The moment $\boldsymbol{M}_{fr}$ is defined for two cases: $|\dot{\varphi}_x| = 0$ (case 1), and $|\dot{\varphi}_x| > 0$ (case 2). For case 1, friction opposes the z-moment due to tail loading, maintaining $\boldsymbol{\alpha} = \boldsymbol{0}$ until the upper bound of $M_{fr,x}$ is reached, as defined in Eq. 15, where μ_s is the static friction coefficient and $d_{fr,eff}$ is the effective moment arm due to the foot spacing and force distribution [20].

$$|M_{fr,x}| \le \mu_s|F_{ft,x}|d_{fr,eff}, \quad \boldsymbol{M}_{fr} = \pm\left[|M_{fr,x}| \;\; 0 \;\; 0\right]^T \tag{15}$$

For case 2, $\boldsymbol{M}_{fr}$ opposes the quad's angular velocity, shown in Eq. 16, where μ_d is the dynamic friction coefficient.

$$M_{fr,x} = -\mu_d|F_{ft,x}|d_{fr,eff}\,\mathrm{sgn}(\dot{\varphi}_x), \quad \boldsymbol{M}_{fr} = \left[M_{fr,x} \;\; 0 \;\; 0\right]^T \tag{16}$$

D. Quadrupedal Model – Roll-Angle Rotations

The roll-angle quad model uses a revolute joint to constrain the quad to single-DOF rotation. As a result, only the z-term of the quad's angular velocity and acceleration are non-zero, shown in Eq. 17, along with an $\boldsymbol{R}_Q$ matrix for the roll-rotation and the non-zero components of $\boldsymbol{M}_{jnt}$ (all three components of $\boldsymbol{F}_{jnt}$ can be non-zero, and the linear acceleration at the pivot is zero).

$$\begin{aligned} &\boldsymbol{\omega} = \left[0 \;\; 0 \;\; \omega_z\right]^T, \quad \boldsymbol{R}_Q = \boldsymbol{R}_Z(\varphi_z), \\ &\boldsymbol{\alpha} = \left[0 \;\; 0 \;\; \alpha_z\right]^T, \quad \boldsymbol{M}_{jnt} = \left[M_{jnt,x} \;\; M_{jnt,y} \;\; 0\right]^T \end{aligned} \tag{17}$$

Figure 4 illustrates the free-body diagram for the roll-angle quad model, where $\boldsymbol{M}_\delta$ is the destabilizing disturbance loading, $\boldsymbol{F}_{C,ft} = [F_{C,ft,x} \;\; 0 \;\; 0]^T$ is the foot contact force when $\varphi_z = 0$, and $\boldsymbol{p}_{JC}$, $\boldsymbol{p}_{JB}$, and $\boldsymbol{p}_{JF}$ are position vectors from the roll joint to the quad COM, tail base frame and $\boldsymbol{F}_{C,ft}$ application point, respectively. The resulting governing equations of motion relative to the joint are defined in Eqs. 18 and 19. Definitions for m, $\boldsymbol{I}$, $\boldsymbol{F}_{tail}$, $\boldsymbol{F}_{grv}$, $\boldsymbol{F}_{T,grv,i}^B$ and $\boldsymbol{M}_{tail}$ match section II-C using $\boldsymbol{R}_Q$ from Eq. 17. The positions $\boldsymbol{p}_{JC}$ and $\boldsymbol{p}_{JB}$ are defined in Eq. 20 using constant vectors in the quad frame.

$$m\left(\tilde{\boldsymbol{\alpha}} + \tilde{\boldsymbol{\omega}}\tilde{\boldsymbol{\omega}}\right)\boldsymbol{p}_{JC} = \boldsymbol{F}_{jnt} + \boldsymbol{F}_{C,ft} + \boldsymbol{F}_{tail} + \boldsymbol{F}_{grv} \tag{18}$$

$$\left(\boldsymbol{I} - m\tilde{\boldsymbol{p}}_{JC}\tilde{\boldsymbol{p}}_{JC}\right)\boldsymbol{\alpha} = \begin{pmatrix} \boldsymbol{M}_{jnt} + \boldsymbol{M}_{tail} + \boldsymbol{M}_\delta \\ + \tilde{\boldsymbol{p}}_{JC}\boldsymbol{F}_{grv} + \tilde{\boldsymbol{p}}_{JB}\boldsymbol{F}_{tail} + \tilde{\boldsymbol{p}}_{JF}\boldsymbol{F}_{C,ft} \end{pmatrix} \tag{19}$$

$$\boldsymbol{p}_{JC} = \boldsymbol{R}_Q\boldsymbol{p}_{JC}^Q, \quad \boldsymbol{p}_{JT} = \boldsymbol{R}_Q\boldsymbol{p}_{JT}^Q \tag{20}$$

The disturbance $\boldsymbol{M}_\delta$ is modeled as a half-sinusoid applied over the first half second of a simulation, with magnitude $M_{\delta,mag}$, as defined in Eq. 21.

$$\boldsymbol{M}_\delta = \begin{cases} M_{\delta,mag}\boldsymbol{z}\sin(\pi t), & 0 \le t \le 0.5 \\ 0, & t > 0.5 \end{cases} \tag{21}$$

E. Quadrupedal Model –Pitch-Angle Rotations

The pitch-angle quad model is similar to the roll-angle model, but the back edge of the rear feet is defined as the revolute joint instead of the left side edge. This leads to alternative definitions of $\boldsymbol{\omega}$, $\boldsymbol{\alpha}$, $\boldsymbol{R}_Q$, and $\boldsymbol{M}_{jnt}$ in Eq. 22.

$$\begin{aligned} &\boldsymbol{\omega} = \left[0 \;\; \omega_y \;\; 0\right]^T, \quad \boldsymbol{R}_Q = \boldsymbol{R}_Y(\varphi_y), \\ &\boldsymbol{\alpha} = \left[0 \;\; \alpha_y \;\; 0\right]^T, \quad \boldsymbol{M}_{jnt} = \left[M_{jnt,x} \;\; 0 \;\; M_{jnt,z}\right]^T \end{aligned} \tag{22}$$

Figure 5 illustrates free-body diagrams for the pitch-angle

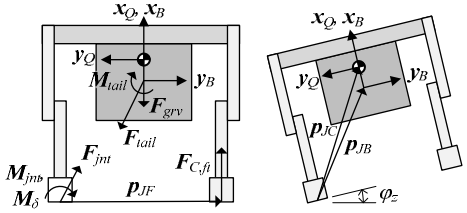

Figure 4. Roll-angle model free-body diagram.

quad model, where $\boldsymbol{F}_{C,tail}$ is the contact force between the tail and ground and $\boldsymbol{p}_{JCT}$ is the position vector from the revolute joint to the tail contact point. The governing equations are defined in Eqs. 23 and 24, and utilize the same formulations as the roll-angle model for m, $\boldsymbol{I}$, $\boldsymbol{F}_{tail}$, $\boldsymbol{F}_{grv}$, $\boldsymbol{F}^{B}_{T,grv,i}$ $\boldsymbol{M}_{tail}$, $\boldsymbol{M}_{\delta}$, $\boldsymbol{p}_{JC}$ and $\boldsymbol{p}_{JB}$. For these calculations, $\boldsymbol{R}_Q$ in Eq. 22 should be utilized, along with the pitch-angle model specific parameters. For $\boldsymbol{M}_{\delta}$, the y-component is time-varying.

$$m\left(\tilde{\boldsymbol{\alpha}}+\tilde{\boldsymbol{\omega}}\tilde{\boldsymbol{\omega}}\right)\boldsymbol{p}_{JC}=\boldsymbol{F}_{jnt}+\boldsymbol{F}_{C,ft}+\boldsymbol{F}_{C,tail}+\boldsymbol{F}_{tail}+\boldsymbol{F}_{grv} \quad (23)$$

$$\left(\boldsymbol{I}-m\tilde{\boldsymbol{p}}_{JC}\tilde{\boldsymbol{p}}_{JC}\right)\boldsymbol{\alpha}=\begin{pmatrix}\boldsymbol{M}_{jnt}+\tilde{\boldsymbol{p}}_{JF}\boldsymbol{F}_{C,ft}+\tilde{\boldsymbol{p}}_{JCT}\boldsymbol{F}_{C,tail}\\+\boldsymbol{M}_{tail}+\tilde{\boldsymbol{p}}_{JB}\boldsymbol{F}_{tail}+\tilde{\boldsymbol{p}}_{JC}\boldsymbol{F}_{grv}+\boldsymbol{M}_{\delta}\end{pmatrix} \quad (24)$$

III. Controller Design

This sections describes the controllers used for yaw-angle maneuvering (III-A) and stabilization in the roll-angle (III-B) and pitch-angle (III-C) directions.

A. Yaw-Angle Maneuvering

For yaw-angle maneuvering, given initial and desired headings, the required action is a net system rotation $\varphi_{rot,des}$. For a given system, there is a maximum angle $|\varphi_{max}|$ the system can rotate due to a single tail motion based on joint angle acceleration limits; therefore, for a given $\varphi_{rot,des}$, the controller will determine whether a single tail motion or multiple tail motions should be used.

1) Single-Motion Tail Maneuvering

If $|\varphi_{rot,des}| < |\varphi_{max}|$, a single tail motion is sufficient to perform the rotation. In order to parameterize the tail motion, split-cycle frequency modulation (SSFM) will be used to generate joint trajectories [20]. In brief, SSFM specifies different sinusoidal half-periods for the acceleration and deceleration phases of the joint angle acceleration. By doing this, the friction loading can be used like a high-pass filter to minimize system acceleration in the undesired direction during that phase of the tail's joint accelerations.

Equation 25 defines the acceleration profile for a given tail motion using three parameters: the joint displacement $\Delta\theta$, the period ΔT and the split-cycle parameter w_{ss}. For a given $\varphi_{rot,des}$, the yaw-angle maneuvering controller will calculate the tail's required SSFM parameters.

$$\ddot{\theta}=\begin{cases}A\sin\left(\pi t/\Delta_1\right) & 0\le t\le\Delta_1\\ -B\sin\left(\pi\left(t-t_{ss}\right)/\Delta_2\right) & \Delta_1<t\le\Delta T\end{cases} \quad (25)$$

$$\Delta_1=w_{ss}\Delta T,\quad \Delta_2=\Delta T-\Delta_1,\quad A=\frac{\pi\Delta\theta}{\Delta_1\Delta T}\quad B=\frac{\pi\Delta\theta}{\Delta_2\Delta T} \quad (26)$$

For this case study, the split cycle and joint displacement are fixed as w_{ss} = 0.2 and $\Delta\theta$ = 30°, leaving ΔT as the variable parameter. Because of the non-linear effect of ground contact friction on the resulting φ_x, a look-up table will be generated through simulations to map ΔT into $\varphi_{rot,des}$, to enable selection of ΔT for a given $\varphi_{rot,des}$. This look-up table will be presented in section IV-B.

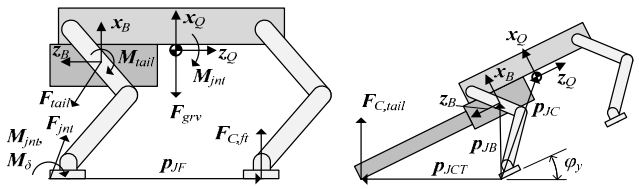

Figure 5. Pitch-angle model free-body diagram.

After performing the planned tail motion, the heading error can be evaluated, and if this error is greater than a prescribed error threshold, a second tail motion can be utilized as a 'fine' adjustment after the 'course' initial pulse.

2) Multiple-Motion Tail Maneuvering

For the case in which a single tail motion is insufficient to generate $\varphi_{rot,des}$, several successive tail actions can be used to achieve the desired rotation. By taking the integer ceiling of the quotient $\varphi_{rot,des}/\varphi_{max}$, the minimum number of tail motions to achieve the desired rotation can be found. However, if the modulus of $\varphi_{rot,des}/\varphi_{max}$ is greater than $0.95\varphi_{max}$, an additional tail motion should be added to allow for modulation of individual desired joint angles as a mechanism for feedback compensation. Therefore, to rotate by $\varphi_{rot,des}$, n tail motions actuating $\Delta\varphi = \varphi_{rot,des}/n$ per tail motion are the planned inputs.

However, as the system rotates, the measured rotation of the system should be compared to the actual rotation. If they differ, the subsequent tail motions should be adjusted to compensate for the error already present, and the known deficiency in a single motion. The modulus check ensures space between $\Delta\varphi$ and φ_{max} for this modification.

B. Roll-Angle Stabilization

For roll-angle stabilization, the goal is to minimize the duration and magnitude of deviation from the stable $\varphi_z = 0$ condition. Therefore, a PD-type controller will be utilized, generating a control input based the system rotation φ_z and its derivative $\dot{\varphi}_z$.

In the tail's workspace, there will be a configuration ($\theta_{seg1,rollMax}$, $\theta_{seg2,rollMax}$) at which the tail COM is the greatest distance from the xz-plane. This configuration leads to the greatest gravitational moment $M_{z,grv,max}$ with respect to the z-axis. Using a search algorithm over the ranges $\theta_{seg1,i}$, $\theta_{seg2,i} \in$ [0, 15°], ($\theta_{seg1,rollMax}$, $\theta_{seg2,rollMax}$) is calculated.

The controller should be able to adjust the tail configuration to a specific z-axis gravitational moment $M_{z,grv}$. Therefore, a locus of tail configurations representing a linear mapping between an input variable $u_M \in$ [-1, 1] and $M_{z,grv} \in$ [$-|M_{z,grv,max}|$, $|M_{z,grv,max}|$] is found. By symmetry, finding a map from $u_M \in$ [0, 1] into $M_{z,grv} \in$ [0, $|M_{z,grv,max}|$] is sufficient for this analysis.

For the desired linear map, define $\theta_{seg1,i}$ and $M_{z,grv}$ according to Eq. 27. With these, only a trajectory for $\theta_{seg2,i}$ is needed that satisfies Eq. 28, where $\boldsymbol{M}_{grv}$ is the total tail gravitational moment and $\boldsymbol{p}_{T,COM}$ is the tail COM position. Based on the definition of $\boldsymbol{p}_{T,COM,i}$ in Eq. 3, it is clearly a function of $\theta_{seg2,i}$, and can be solved inversely for $\theta_{seg2,i}$ given a desired $\boldsymbol{p}_{tail,COM}$ (calculated from $M_{z,grv}$) and $\theta_{seg1,i}$.

$$\theta_{seg1,i}=\theta_{seg1,rollMax}u_M,\quad M_{z,grv}=M_{z,grv,max}u_M \quad (27)$$

$$\boldsymbol{M}^{B}_{T,grv}=\sum_{i=0}^{12}\left(\tilde{\boldsymbol{p}}^{B}_{BT,COM,i}\boldsymbol{F}^{B}_{T,grv,i}\right),\quad M_{grv,z}=\left(\boldsymbol{z}^{B}_{B}\right)^{T}\boldsymbol{M}^{B}_{T,grv} \quad (28)$$

A control law is needed to map φ_z and $\dot{\varphi}_z$ into u_M. A saturation-limited PD control law is defined in Eq. 29, where K_P and K_D are proportional and derivative control gains, and

sat() is the unit saturation function. The saturation prevents the control action from exceeding its bounds.

$$u_M = \text{sat}\left(-K_P\varphi_z - K_D\dot{\varphi}_z\right), \quad \text{sat}(x) = \begin{cases} x & |x| \le 1 \\ x/|x| & |x| > 1 \end{cases} \tag{29}$$

C. Pitch-Angle Stabilization

Pitch angle stabilization in the positive pitch direction is not due to any control action applied by the tail—it is merely due to the presences of the tail. Assume the case study under consideration is backward pitching due to $\boldsymbol{M}_\delta$ (forward pitching would require $\boldsymbol{M}_\delta$ to overcome the combined gravitational moment due to the quad and tail). As shown in Fig. 5, at the 'kickstand' angle $\varphi_y = \varphi_k$, the tail will contact the ground. This will generate a force $\boldsymbol{F}_{C,tail}$ between the ground and the terminal tail disk. This force will oppose $\boldsymbol{\alpha}$ and $\boldsymbol{M}_\delta$, driving the former to zero and providing a moment equal and opposite to $\boldsymbol{M}_\delta$ while $\|\boldsymbol{M}_\delta\| > 0$.

While in this 'kickstand' mode, one of two cases will occur once $\boldsymbol{\alpha} = \boldsymbol{0}$ and $\boldsymbol{M}_\delta = \boldsymbol{0}$: (1) the system will fall back to its stable standing configuration, or (2) the system will remain leaning against the tail. Case 1 will occur when the system COM is in front of the pivot, and case 2 will occur when the system COM is behind the pivot.

For case 1, no further action is necessary to stabilize the robot: it will naturally fall forward and regain ground contact. However, for case 2, a control algorithm can be generated to generate a tail trajectory to assist in righting the system bending the tail downward to push against the ground. The system under consideration in section IV belongs to case 1.

IV. Case Studies

This section describes the implementation of the control algorithms in virtual simulations of the yaw (IV-B), roll (IV-C) and pitch (IV-D) case studies, after presenting the simulation parameters used for these simulations (IV-A).

A. Simulation Parameters

Tables 1 and 2 present the shared modeling parameters for the tail and quad for all three simulations, and Table 3 presents the simulation-specific parameters. Given the relatively small size of the tail links in relation to the quadruped, they are modeled as point masses.

B. Yaw-Angle Maneuvering

Two case studies are considered, matching the subsections in section III-A: a single-motion maneuver, and a multiple-motion maneuver. First, however, a map between $\varphi_{rot,des}$ and ΔT is generated using the yaw-angle rotation model. Figure 6 illustrates this map, for a net rotation range of 0 to 25°.

The two case studies will be generated for desired rotations of 21° and 63°. For the single-motion 21° rotation, the planned ΔT = 0.6427 s, and the resulting system trajectory is plotted in Fig. 7(a). The final φ is 21.09°, a negligible error. For the multiple-motion 63° rotation, three 21° motions are initially planned. As shown in Fig. 7(b), after the first motion, the first intermediate φ is 21.09°, and the second tail motion is adjusted to 20.82° (ΔT = 0.6448 s) to compensate for the previous error and the predicted error

TABLE I. Tail Properties

Variable	Value	Variable	Value
$L_{JJ,0}$	170 mm	$I^B_{T,0,xx}$	0.0225 kg-m
L_{JJ}	40 mm	$I^B_{T,0,yy}$	0.0202 kg-m^2
L_{JC}	31.8 mm	$I^B_{T,0,zz}$	0.0050 kg-m^2
$m_{T,0}$	3.96 kg	$\boldsymbol{I}^B_{T,\{1\text{–}12\}}$	**0** kg-m^2
$m_{T,\{1\text{-}12\}}$	0.7 kg		

TABLE II. Shared Quad Properties

Variable	Value	Variable	Value
m_Q	21.64 kg	$\boldsymbol{I}^Q_{Q,xx}$	1.1534 kg-m^2
$\boldsymbol{I}^Q_{Q,yy}$	1.0062 kg-m^2	$\boldsymbol{I}^Q_{Q,zz}$	0.7533 kg-m^2

TABLE III. Simulation-Specific Properties

Yaw Simulation			
Variable	***Value***	***Variable***	***Value***
$\boldsymbol{p}^Q_{QT}$	[-60.32; 0; -96.7] mm	$d_{fr,eff}$	240 mm
μ_s	0.3	μ_d	0.25
Roll Simulation			
Variable	***Value***	***Variable***	***Value***
$\boldsymbol{p}^Q_{JC}$	[322; -245; 0] mm	$\boldsymbol{p}^Q_{JT}$	[262; -245; -96.7] mm
$\boldsymbol{p}_{JF}$	[0; -430; 0] mm	$M_{\delta,mag}$	110 N-m
Pitch Simulation			
$\boldsymbol{p}^Q_{JT}$	[262; 0; 119] mm	$\boldsymbol{p}^Q_{JC}$	[322; 0; 216] mm
$\boldsymbol{p}_{JF}$	[0; 0; 373] mm	$\boldsymbol{p}_{JCT}$	[0; 0; -579.76] mm
φ_k	23.91°	$M_{\delta,mag}$	220 N-m

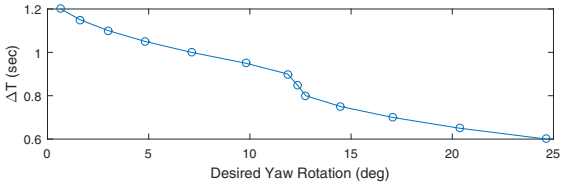

Figure 6. Yaw-angle ΔT calculating based on desired φ_x.

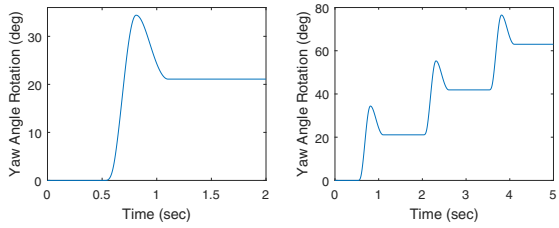

Figure 7. Yaw-angle trajectories for (a) single-motion, (b) multiple-motion case studies.

for this tail motion. After the second motion, the second intermediate φ is 41.89°, and the final tail motion is adjusted to 21.18° (ΔT = 0.6406 s). After the third motion, the final φ = 63° has reached the desired heading.

C. Roll-Angle Stabilization

For this case study, the use of the tail should demonstrate the ability to stabilize a system that the applied disturbance would otherwise destabilize. Figure 8 compares the response of a system with and without control action (K_P = 0.3 and K_D = 0.025 s). As shown, without the control action, $\boldsymbol{M}_\delta$ causes the system COM to cross the x-z plane at the joint, resulting in destabilization, whereas the control action sufficiently

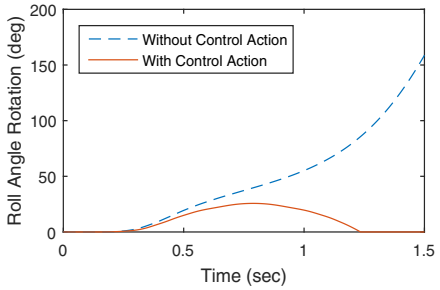

Figure 8. Effect of roll-angle control action.

counteracts that disturbance to prevent tipping.

Increasing K_P and K_D have similar effects: they impede the further undesired rotation of the quadruped, up to the saturation limit. In this system, given the relative tail mass versus the quadruped mass, the tail is driven to its maximum loading position in order to resist the disturbance. Further optimization of the tail mass in relation to the quadruped inertia, along with exploring the use of dynamic loading with the tail's roll angle will be elements of future work.

D. Pitch-Angle Stabilization

Figure 9 shows the impact of tail-ground contact on stopping the rotation due to a pitching disturbance. At the kickstand angle φ_k, the tail stops the system's rotation. The tail remains in contact while the disturbance overcomes the gravitational moment, but the system falls back to its stable configuration after the disturbance is sufficiently reduced.

V. Conclusion

This paper has demonstrated the R3RT's fundamental capabilities of assisting in the maneuvering and stabilization of a quadrupedal robot. Numerical simulations have demonstrated the tail's utility in generating yaw-angle rotation for turning the robot and rejecting external disturbances to prevent the robot from tipping in the pitch and roll directions. Ongoing and future work will formulate a single dynamics model for the full six-DOF system behavior that incorporates the cable-driven R3RT dynamics. Inner-loop controllers to prescribe desired motor torques to the actuation module will be used to more accurately simulate the experimental system behavior. Stabilization loading utilizing the tail roll will also be considered alongside the approach utilizing gravitational loading presented in this paper. Finally, refinements to the design of the tailed quadruped system will be applied to reduce system mass and inertia to improve the effectiveness of the tail.

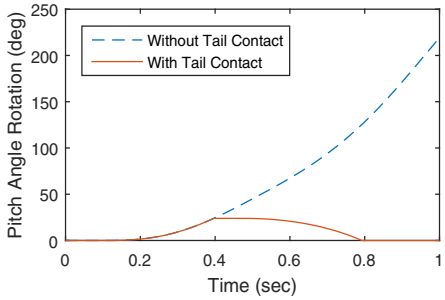

Figure 9. Pitch-angle rotation stabilizaion due to tail presence.

References

[1] P. J. Csonka and K. J. Waldron, "A Brief History of Legged Robotics," in *Technology Developments: the Role of Mechanism and Machine Science and IFToMM*, 2011, pp. 59–73.

[2] J. Or, "Humanoids Grow a Spine," *IEEE Robotics and Automation Magazine*, no. June, pp. 71–81, 2013.

[3] S. Seok, A. Wang, M. Y. Chuah, D. Otten, J. Lang, and S. Kim, "Design Principles for Highly Efficient Quadrupeds and Implementation on the MIT Cheetah Robot," in *IEEE International Conference on Robotics and Automation*, 2013, pp. 3307–3312.

[4] G. C. Hickman, "The Mammalian Tail: a Review of Functions," *Mamm. Rev.*, vol. 9, no. 4, pp. 143–157, 1979.

[5] C. Walker, C. J. Vierck Jr., and L. A. Ritz, "Balance in the Cat: Role of the Tail and Effects of Sacrocaudal Transection," *Behav. Brain Res.*, vol. 91, pp. 41–47, 1998.

[6] A. M. Wilson, J. C. Lowe, K. Roskilly, P. E. Hudson, K. A. Golabek, and J. W. McNutt, "Locomotion Dynamics of Hunting in Wild Cheetahs.," *Nature*, vol. 498, no. 7453, pp. 185–189, 2013.

[7] S. M. O'Connor, T. J. Dawson, R. Kram, and J. M. Donelan, "The Kangaroo's Tail Propels and Powers Pentapedal Locomotion," *Biol. Lett.*, vol. 10, no. 20140381, 2014.

[8] N. J. Kohut, D. W. Haldane, D. Zarrouk, and R. S. Fearing, "Effect of Inertial Tail on Yaw Rate of 45 Gram Legged Robot," *Int. Conf. Climbing Walk. Robot. Support Technol. Mob. Mach.*, pp. 157–164, 2012.

[9] A. Patel and M. Braae, "Rapid Acceleration and Braking: Inspiration from the Cheetah's Tail," in *IEEE International Conference on Robotics and Automation*, 2014, pp. 793–799.

[10] T. Libby, T. Y. Moore, E. Chang-Siu, D. Li, D. J. Cohen, A. Jusufi, and R. J. Full, "Tail-assisted Pitch Control in Lizards, Robots and Dinosaurs.," *Nature*, vol. 481, no. 7380, pp. 181–184, Jan. 2012.

[11] A. Patel and M. Braae, "Rapid Turning at High-Speed: Inspirations from the Cheetah's Tail," in *IEEE/RSJ International Conference on Intelligent Robots and Systems*, 2013, pp. 5506–5511.

[12] A. Mutka, M. Orsag, and Z. Kovacic, "Stabilizing a Quadruped Robot Locomotion Using a Two Degree of Freedom Tail," in *21st Mediterranean Conference on Control and Automation*, 2013, pp. 1336–1342.

[13] F. Ikeda and S. Toyama, "A Proposal of Right and Left Turning Mechanism for Quasi-Passive Walking Robot," in *IEEE International Conference on Advanced Robotics and Intelligent Systems*, 2015.

[14] W. Saab, A. Kumar, W. S. Rone, and P. Ben-Tzvi, "Design and Integration of a Novel Spatial Articulated Robotic Tail," *IEEE Trans. Robot.*, Under Review.

[15] W. S. Rone, W. Saab, and P. Ben-Tzvi, "Design, Modeling and Optimization of the Universal-Spatial Robotic Tail," in *IEEE/RSJ International Conference on Intelligent Robots and Systems*, 2017, Under Review.

[16] W. Saab and P. Ben-Tzvi, "Design and Analysis of a Discrete Modular Serpentine Tail," in *ASME International Design Engineering Technical Conference & Computers and Information in Engineering Conference*, 2016, p. 59387: 1-8.

[17] W. S. Rone and P. Ben-Tzvi, "Multi-Segment Continuum Robot Shape Estimation using Passive Cable Displacement," in *IEEE International Symposium on Robotic and Sensors Environments*, 2013, pp. 37–42.

[18] W. S. Rone and P. Ben-Tzvi, "Continuum Manipulator Statics Based on the Principle of Virtual Work," in *ASME International Mechanical Engineering Congress and Exposition*, 2012.

[19] W. Saab, W. S. Rone, and P. Ben-Tzvi, "Robotic Modular Leg: Design, Analysis and Experimentation," *J. Mech. Robot.*, vol. 9, p. 24501, 2016.

[20] W. S. Rone and P. Ben-Tzvi, "Dynamic Modeling and Simulation of a Yaw-Angle Quadruped Maneuvering with a Robotic Tail," *J. Dyn. Syst. Meas. Control.*, vol. 138, no. 8, p. 084502: 1-7, 2016.

[21] W. S. Rone and P. Ben-Tzvi, "Continuum Robotic Tail Loading Analysis for Mobile Robot Stabilization and Maneuvering," in *ASME International Design Engineering Technical Conference & Computers and Information in Engineering Conference*, 2014.